Ethylcyclohexane Hydroconversion in EU-1 Zeolite: DFT-based Microkinetic Modeling Reveals the Nature of the Kinetically Relevant Intermediates

Ester Gutierrez-Acebo, Jerome Rey, Christophe Bouchy, Y. Schuurman, Céline Chizallet

Ethylcyclohexane Hydroconversion in EU-1 Zeolite: DFT-based Microkinetic Modeling Reveals the Nature of the Kinetically Relevant Intermediates

Ester Gutierrez-Acebo,[a] Jérôme Rey,[a] Christophe Bouchy,[a] Yves Schuurman,*[b] and Céline Chizallet*[a]

The transformation of cycloalkanes is a key-reaction in refining and petrochemistry. Herein, we unravel the mechanism and the kinetics of the transformation of ethylcyclohexane, considering a bifunctional catalyst composed of platinum and of the EU-1 zeolite, by experiments, density functional theory (DFT) calculations and DFT-based microkinetic modeling. The simulated mechanisms involve carbenium intermediates. DFT shows the central kinetic role of the π-complexes corresponding to secondary carbenium ions. Cycle contractions and expansions appear to be rate-limiting. The DFT-based microkinetic model includes a limited number of kinetic parameters optimized by regression with respect to the experimental data. The agreement with experimental results is very good, showing that the mechanisms proposed, the nature of the intermediates, and the values of the computed rate constants, are relevant. The reaction starts by the cycle contraction of 1-ethylcyclohexene, then shifts to a second sequence of cycle expansion-contraction reactions by intercalated methyl-shifts.

Introduction

The prediction of the catalyst properties, in particular in terms of selectivity, is a current challenge. Whereas first principles calculations provide precious mechanistic insights and offer the possibility to quantify rate constants for elementary steps, the quantification of the whole reaction rate is sometimes tricky when the number of competitive elementary reaction steps becomes significant. This is typically the case for the transformation of hydrocarbons by zeolites, usually consisting in a large set of elementary steps, many of them playing a role in the final selectivity.[1,2] In such a case, the help of multiscale modeling, consisting in feeding microkinetic models by first principles data, is a significant step forward in the quantification of the rate and selectivities, in order to be directly compared with experiments. Such an approach appeared to be successful in several cases,[3] a few of them related to catalysis by zeolites, with variable degree of success in selectivity predictions.[4]

The isomerization and cracking of alkanes is of paramount relevance in refining and petrochemistry, *inter alia*.[1,5] The atomic scale mechanisms of the transformation of cycloalkanes (naphthenes) have been, however, far less investigated with respect to paraffins. These reactions are usually performed in the context of bifunctional catalysis, where a metallic phase dehydrogenates cycloalkanes into cycloalkenes, themselves transformed by an acid phase, usually a zeolite.[6,7] The desired isomerization reactions are usually considered to take place via carbenium chemistry,[1,8] which was confirmed theoretically.[9] Notably, in the industrial context of ethylbenzene isomerization into xylenes, the metallic phase hydrogenates the aromatic ring, until a cycloalkene is formed. The latter is then transformed at the zeolite Brønsted acid sites[1,10] into different carbocations which will be finally dehydrogenated into the different xylenes. Although the starting points differ (cycloalkane *versus* substituted aromatic molecule), the reactions taking place at the acid sites are the same. For this reason, we focus in the present work on the isomerization mechanism of ethylcyclohexene in the EU-1 zeolite. The latter is used at the industrial scale for ethylbenzene hydroisomerization.[10]

Thus, in order to unravel these mechanisms, we combine experiments dealing with the kinetics of the ethylcyclohexane (ECH) transformation reactions, recorded on a well-balanced bifunctional catalyst[11] (meaning in conditions where the reactions taking place at the acid phase are limiting, whereas reactions taking place at the metallic phase are at thermodynamic equilibrium[8]), with first principles calculations that then feed a microkinetic model. In a preliminary study, we have established the apparent reaction scheme[11] (Scheme 1). It starts by ECH isomerization reactions into ethyl-methyl-cyclopentanes (EMCP), then dimethylcyclohexanes (DMCH), then trimethylcyclopentanes (TMCP). Isomerization products also give rise to undesired (in the context of ethylbenzene isomer-

[a] *Dr. E. Gutierrez-Acebo, Dr. J. Rey, Dr. C. Bouchy, Dr. C. Chizallet*
IFP Energies Nouvelles
Rond-Point de l'échangeur de Solaize BP3
F-69360, Solaize (France)
E-mail: celine.chizallet@ifpen.fr
[b] *Dr. Y. Schuurman*
CNRS, UMR 5256, IRCELYON, Institut de recherches sur la catalyse et l'environnement de Lyon
Université Lyon 1
2 Avenue Albert Einstein
F-69626, Villeurbanne (France)
E-mail: yves.schuurman@ircelyon.univ-lyon1.fr

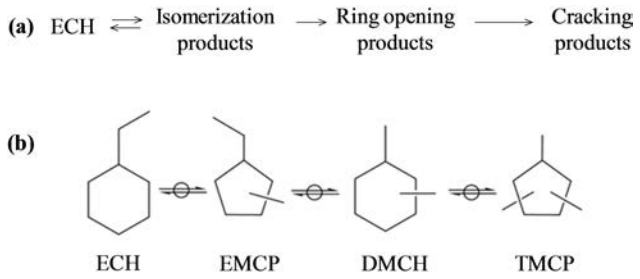

Scheme 1. Ethylcyclohexane hydroconversion; apparent reaction scheme (a) and apparent isomerization reaction scheme (b). Adapted from Ref. [11].

ization) ring opening products, that very quickly yield cracking products (alkanes with less than 8 carbon atoms). Notably, the isomerization is expected to take place between unsaturated forms of the cyclo-alkanes represented in Scheme 1, that are re-hydrogenated before experimental detection of the isomerized and cracked products.

We have also elucidated the part of the reaction network, that occurs only through tertiary carbenium intermediates.[9] In the present work, we extend the network to secondary carbenium species too, as tertiary carbenium ions are not sufficient to describe the variety of experimentally observed isomerization products.[11] In our first principles calculations, we will focus on the active sites located in the 10 MR channels of the EU-1 zeolite, as these were shown to be among most active sites in the EUO framework (in contrast with sites located at the intersection between the 10 MR channels and 12 MR side pockets).[9] Herein, we show that the synergy between experiments, periodic density functional theory (DFT) calculations and microkinetic modeling is key to conclude about the most relevant reaction steps and intermediates, and to quantify the corresponding rate constants.

Results and Discussion

ECH conversion: experimental features

Experimentally, we investigated the bifunctional transformation of ethylcyclohexane (ECH) over a 1 wt.% Pt/γ-Al_2O_3-H-EU-1 catalyst, composed of a mechanical mixture of platinum supported on gamma-alumina and protonic EU-1 (H-EU-1) zeolite. It was shown to be a well-balanced catalyst,[11] thus the kinetic limitations are due to reactions taking place at the zeolite acid sites only. The evolution of the conversion and selectivity *versus* the contact times was measured, as well as lumped selectivities into the various families of isomers observed (Figure 1). The conversion increases with contact time and with temperature, while the ring opening and cracking selectivities do not change with the temperature for a given conversion (Figure S1). The isomerization and dehydrogenation selectivities change slightly for a given conversion when the temperature is increased: isomerization selectivity decreases whereas dehydrogenation selectivity increases. This subtle

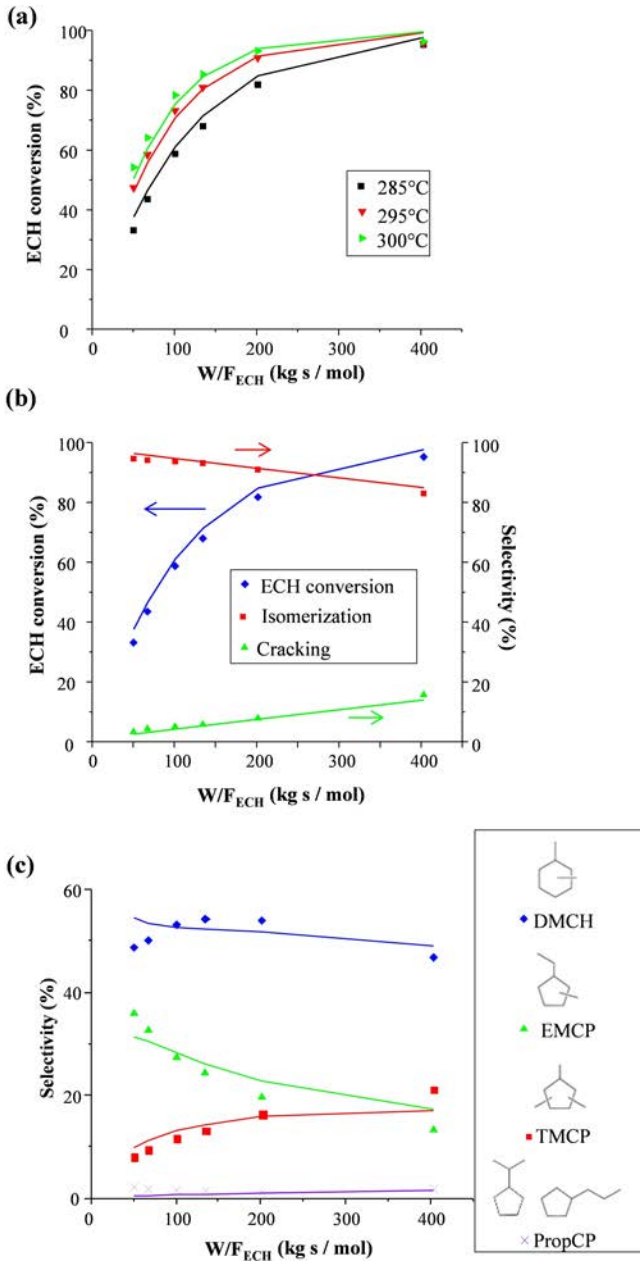

Figure 1. (a) ECH conversion *versus* contact time (catalyst mass W divided by the ECH flow F_{ECH}), for three temperatures. (b) ECH conversion and selectivity *versus* contact time at 285 °C. (c) Selectivities in lumped isomers families *versus* contact time at 285 °C. Full lines: kinetic modeling data; dots: experimental data.

change in isomerization and dehydrogenation selectivities is explained by the fact that at higher temperatures, the equilibrium shifts further towards the dehydrogenation products. Then, the loss of isomerization selectivity results in a gain on the dehydrogenation selectivity (dehydrogenation of the isomerization products). As these changes remain marginal, the evolution of the products selectivities with conversion and contact time are represented for a single temperature, 285 °C (Figure 1-b, c).

Figure 1-b confirms that the primary products are the isomerization ones since they are the only products appearing at low ECH conversion. The ring opening and dehydrogenation products are almost inexistent, whereas the amount of cracking products increases as the contact time increases. This confirms the apparent reaction mechanism proposed in Scheme 1. The very low amount of ring opening products is due to the fact that they are immediately transformed into cracked products.

In order to study the isomerization kinetics, the selectivities in the isomers lumped in their different families are monitored experimentally at different ECH conversions (varying the contact time) at 285 °C (Figure 1-c). The observed trend is again fully compatible with the apparent reaction scheme proposed in Scheme 1. Propylcyclopentanes (PropCP) are detected in very low amount, explaining why they are not appearing in the main reaction scheme.

Figure 2 reports more detailed data in terms of selectivities in the various isomers. In Figures S2-S4, the data are depicted in terms of mole fraction of each component within a family, together with thermodynamic equilibrium data for comparison. Within the EMCP family (Figure 2-a), 1-ethyl,3-methyl-cyclopentanes (13-EMCP) appear as the major primary products. 1-ethyl,2-methyl-cyclopentanes (12-EMCP) appear in lower amount, whereas 1-ethyl,1-methyl-cyclopentane (11-EMCP) slightly increases with contact time. Within the DMCH family (Figure 2-b), 1,4-dimethyl-cyclohexanes (14-DMCH) and 1,3-dimethyl-cyclohexanes (13-DMCH) are the main and primary products (although the exact amount of 13-DMCH is likely underestimated, that of 14-DMCH overestimated, for reasons explained in Supporting Information S1). The amounts of 1,2-dimethyl-cyclohexanes (12-DMCH) and 1,1-dimethyl-cyclohexane (11-DMCH) remain lower on the whole ECH conversion range. Finally, within the TMCP family (Figure 2-c), 1,2,4-trimethyl-cyclopentanes (124-TMCP) are the dominant products, followed by 1,1,3-trimethyl-cyclopentane (113-TMCP) and 1,2,3-trimethyl-cyclopentane (123-TMCP). 1,1,2-trimethyl-cyclopentane (112-TMCP) appears in lower amount. Thus, the order of isomers appearance in each lump can be depicted as shown in Scheme 2. Concerning the primary isomerization products family (EMCP), the 13-EMCP appears first, followed by 12-EMCP and at last, 11-EMCP. Consecutively, the DMCH family has 13-DMCH and 14-DMCH as first products appearing, followed by 12-DMCH and 11-DMCH at last. Regarding the TMCP family, the first isomer appearing is the 124-TMCP followed by 113-TMCP and 123-TMCP and 112-TMCP appearing at last. Note that for the EMCP and TMCP family the order of appearance of the isomers is in accordance with successive carbon to carbon methyl shift. For the DMCH family, it is not possible to conclude whether 13- or 14-DMCH appears first. From this product analysis the possible isomerization mechanism paths will be investigated by DFT.

The distribution of ring opening and cracking products is reported for the effluent composition obtained at 300 °C at a contact time of 101 kg s/mol (Figure 3). This temperature has been chosen in order to have significant amount of cracking and ring opening products in the effluent (1.16 wt.% of ring opening and 5.6 wt.% of cracking products).

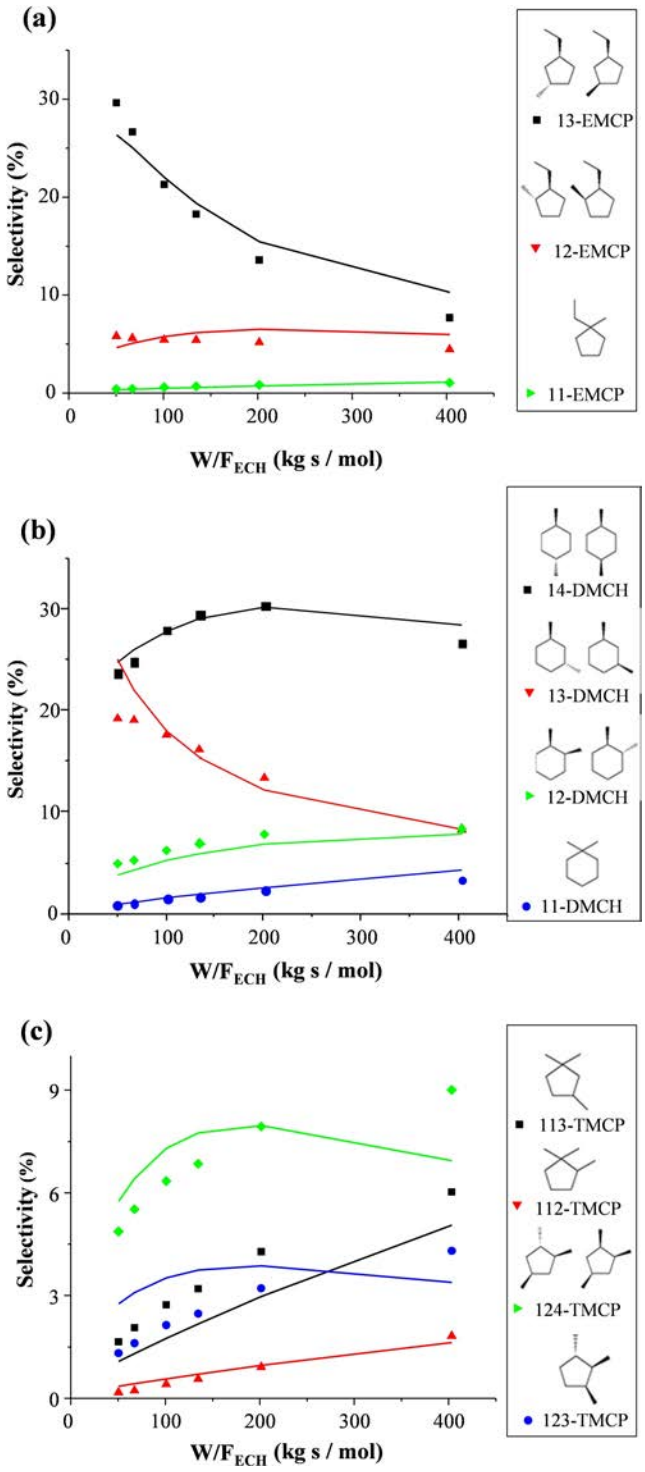

Figure 2. Selectivities in the various isomers obtained *versus* contact time at 285 °C. Full lines: kinetic modeling data; dots: experimental data. (a) EMCP family, (b) DMCH family, (c) TMCP family.

It must be emphasized that the results should be considered cautiously as not all the ring opening products are identified by GC. This is due for instance, to coelution with other compounds during GC analysis (see supporting information of Ref. [11]). The C_8 paraffins are mainly branched ones (n-

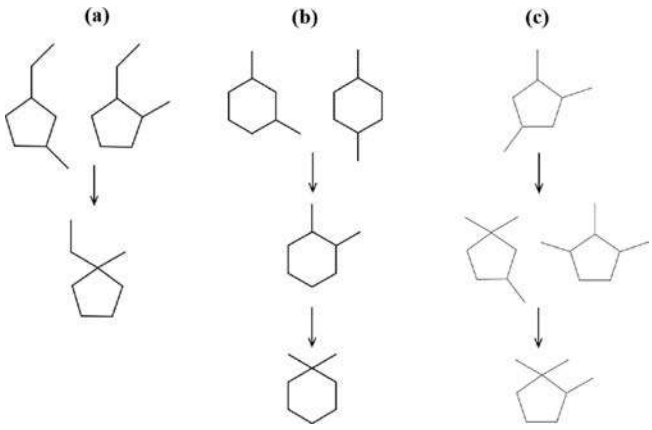

Scheme 2. Isomer apparition order in (a) EMCP family, (b) DMCH family and (c) TMCP family, according to experimental observations.

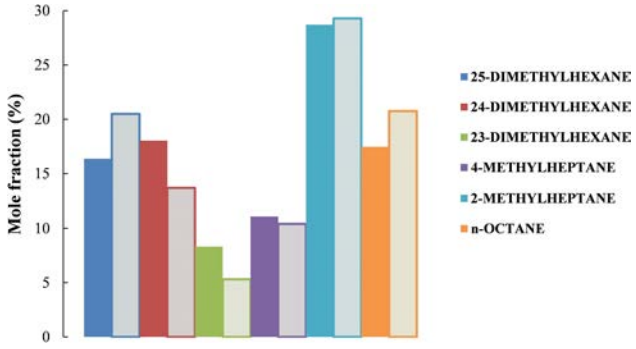

Figure 3. Ring opening (RO) product distribution at 300 °C at a contact time of 101 kg s/mol. in full lines. Ring opening (RO) product distribution at 300 °C calculated with PROII in hatched lines. RO global yield at 300 °C = 1.16 wt.%.

octane stands for only 20% of the identified products). The amounts of monobranched and dibranched products are about the same (about 40%) and no tribranched products are observed. 2-methyl-heptane and 2,5-dimethyl-hexane are the main principal isomerized products: these two molecules represent half of the total identified ring opening products. The ring opening products distribution calculated at thermodynamic equilibrium with PROII (see experimental section), include ring opening isomers not appearing experimentally or appearing in coelution with another products. Thus, in order to compare experimental and PROII results, from PROII results, only the isomers appearing experimentally have been considered and normalized to 100 (hatched line bars in Figure 3). It can be observed that the mono-branched products are close to equilibrium. In the case of the multibranched isomers, 2,4-dimethylcyclohexane and 2,3-dimethylcyclohexane appear in higher amount experimentally than at equilibrium (5 and 3% respectively) whereas 2,5-dimethylcyclohexane appears experimentally lower than at the equilibrium (5%). Concerning the n-octane, experimental amounts are lower than equilibrium.

Assuming that the dominant modes of β-scissions are the ones that transform tertiary carbenium ions into other tertiary carbenium ions, or secondary into tertiary, and tertiary into secondary,[1] it can be expected that 113-TMCP is particularly prone to form the 2,5-dimethyl-hexane by ring opening (tertiary-tertiary β-scission, Scheme 3-a).[1] Following the same guideline, 1,1-dimethyl-cyclohexane or 1,3-dimethyl-cyclohexane can form the 2-methyl-heptane by secondary-tertiary or secondary-tertiary β-scission (Scheme 3-b). Note that the ring opening products may themselves undergo bifunctional isomerization reactions, leading to other mono/di/tribranched products.[12] Concerning the presence of the n-octane product, it could come either from the isomerization of the branched ring opening product or from the opening of a naphthenic ring isomer such as ECH^+ (Figure S5).[7] Nonetheless, the latter possibility seems quite unlikely since n-octane coming from the naphthenic ring opening involves a primary carbocation. In the following DFT study, we will therefore focus on the ring opening pathways described in Scheme 3.

Reaction pathways for the isomerization and ring opening of ethylcyclohexene: DFT results

In order to elucidate the nature of the elementary steps and to provide values for the kinetic constants of each individual step, an first principles investigation of part of the reaction network has been performed, considering the T_1O_1 site located in the 10 MR channel of the EUO structure. The reaction scheme considered for Type B isomerization reactions (resulting in a change of branching degree, here through cycle expansion-contraction steps), related protonation-deprotonation and hydro-dehydrogenation reactions, is depicted in Figure S6. A simplified representation (showing only the carbenium ions) is given in Scheme 4. Some Type A reactions (that do not change the branching degree) were also the object of DFT calculations, but in line with previous experimental and theoretical works,[1,13–15] they are much faster than Type B isomerization reactions, so our main focus among isomerization steps will be put on Type B reactions. Each carbenium ion was connected to a corresponding π-complex (adsorbed alkene form) when the proton is transferred back to the zeolite framework.

A part of Path I (from a) to e)) was investigated in Ref. [9]. Nevertheless, the experimental product distribution makes it clear that this part of the pathway is not sufficient to explain all the reaction products. For example, the formation of 13-EMCP

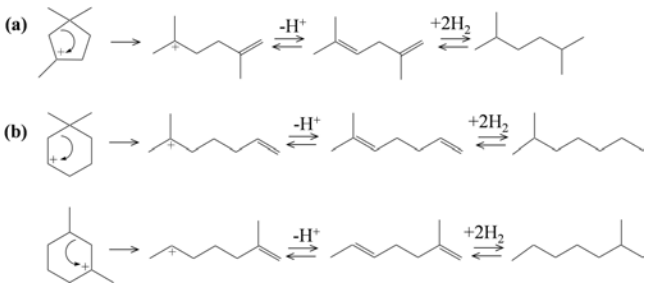

Scheme 3. Ring opening pathway providing a) 2,5-dimethylhexane and b) 2-methylheptane.

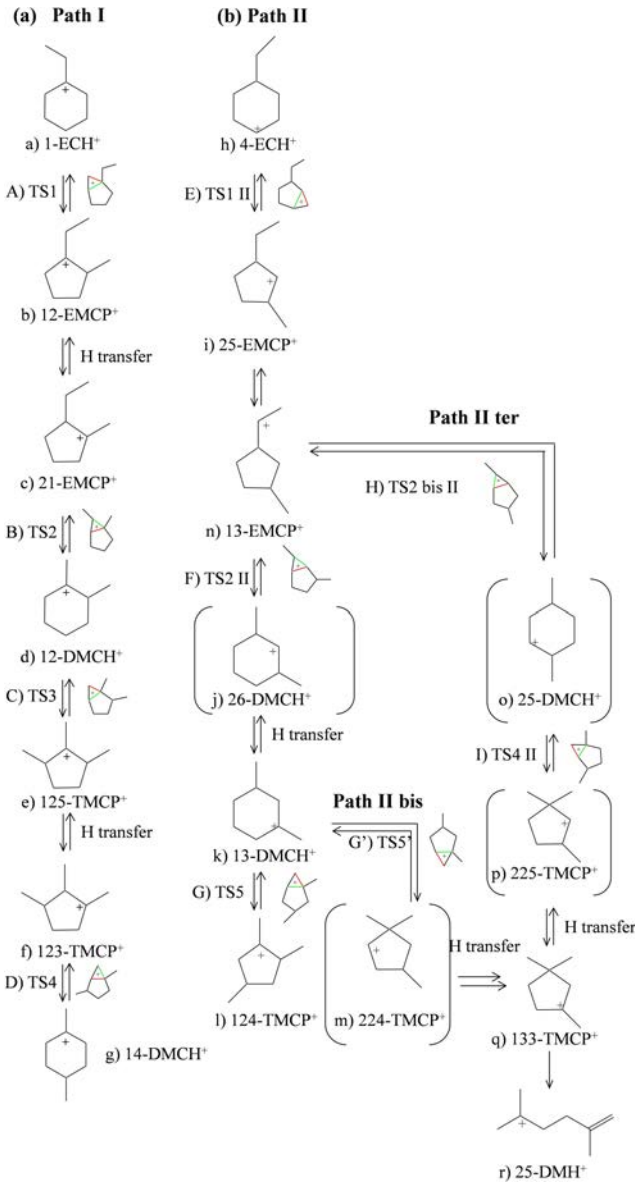

Scheme 4. Simplified Type B isomerization pathways considered in the kinetic study. (a) Path I, (b) Path II and derived pathways. In transition structures, the bond that breaks/forms from the top to the bottom is depicted in red/green, respectively. The full reaction scheme investigated by DFT, reported in Figure S6, also includes protonation/deprotonation reactions linking carbenium ions and π-complexes. Secondary carbenium depicted into brackets could not be optimized as local energy minima, thus the corresponding π-complex was considered in the kinetic modeling.

or 13-DMCH are not explained by the sole Path I. Two hypotheses can be proposed to explain the formation of these compounds:

- Either they are formed from 12-EMCP$^+$/12-DMCH$^+$ by a sequence of hydride and methyl shifts. Such a sequence needs secondary carbenium to appear in the reaction sequence (possible hydride and methyl shifts are reported in Figures S7–S9). This is however not compatible with the experimental observation of 13-EMCP or 13-DMCH (Figure 2) as primary reaction products.
- Either they are formed by another sequence of Type B isomerization reactions. This is featured in Path II, which also requires some secondary carbenium ions to be invoked.

Moreover, Path II bis and II ter were added to account for the formation of 113-TMCP, observed experimentally and thought to be a key intermediate (in its carbenium form, Scheme 3) for ring opening. The nature of the intermediates is also defined from the results of the Intrinsic Reaction Coordinate Analysis performed starting from optimized transition structures, that reveal the most likely reaction routes.

We managed to identify some secondary carbocations as reaction intermediates in some cases. However, some others (depicted into brackets in Scheme 4) appeared not to be local energy minima in the channel of EUO. They are likely on flat areas of a descending potential energy profile.[15,16] The energy of secondary carbenium ions that can be optimized remains very high compared to their corresponding π-complex (Figure S10). Thus, from a kinetic point of view, it can be anticipated that when a secondary carbenium is needed to convert one species in another, the relevant kinetic intermediate will be the corresponding π-complex.

As found previously for the first part of Path I,[9] the transition states found for Type B isomerizations (here cycle contraction-expansion) are edge Protonated Cyclo-Propane ions (PCP). The structure (Table S1) of all intermediates and transition states found is reported in Figures S11, S12 and S13. Examples are given in Figure 4. All the PCP structures exhibit many common features: the C–C bond holding the edge-H is longer (1.7–1.8 Å) than the two other ones of the triangle (1.4–1.6 Å). The edge-H is asymmetrically located between two C atoms (C–H bonds of about 1.2 and 1.5 Å).

The energy and free energy profiles are reported in Figure 5. Table S2 reports the explicit values of all the energies, enthalpies, entropies, and Gibbs free energies at 285 °C. Transition states were connected to the corresponding reactant and products (intermediates of the whole pathway) by an IRC analysis. The stability of the corresponding π-complexes is also given for each carbenium. Path I is likely the first appearing since the energy barrier to reach the first TS (A) for 1-ECH$^+$(a) is 57 kJ/mol and the corresponding π-complex is highly stable ($E_{ads} = -133$ kJ/mol). The first TS of Path II (E) is higher in energy

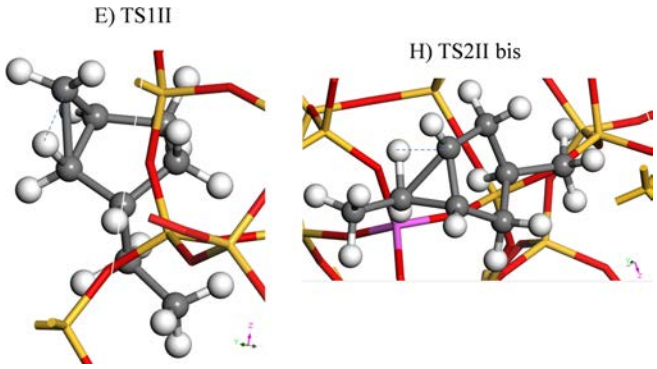

Figure 4. Examples of transition states for Type B isomerization reactions (cycle contraction-expansion steps) determined by DFT.

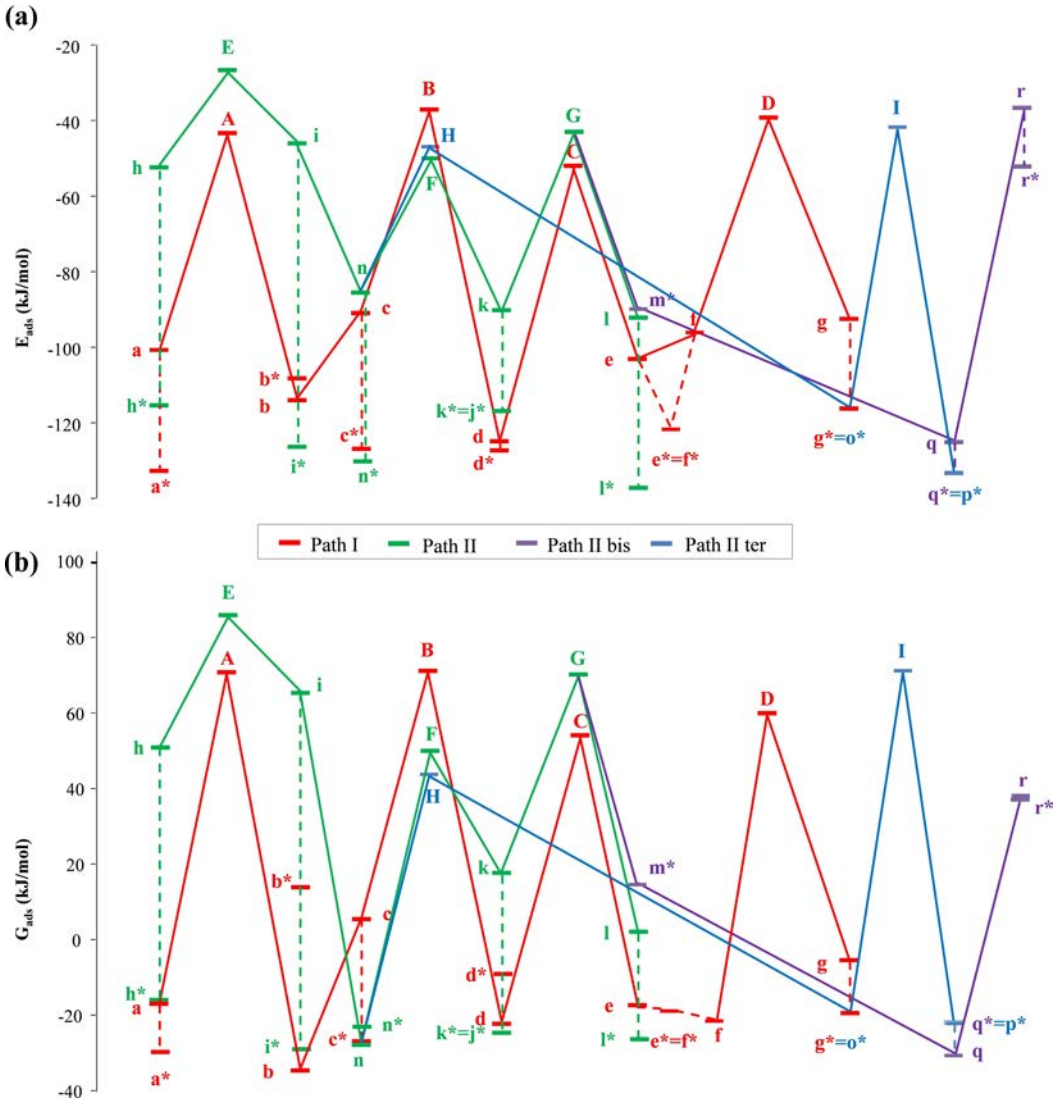

Figure 5. Energy (a) and Gibbs free energy diagrams at 285 °C (b) for the Type B isomerization sequence (plus ring opening, q→r). Stars depict π-complexes with the same skeleton as related carbenium ions. r* is the diene depicted in Scheme 3-(a).

and free energy than A (G_{ads} = 86 *versus* 71 kJ/mol). Notably, the least stable TS is E, which is the only one not harboring alkyl group on the triangle other than the C5 cycle. For the second steps of paths I and II, the reverse trend can be perceived, F being more stable than B (G_{ads} = 50 *versus* 71 kJ/mol). The structural specificity of F is that it harbors a methyl group on the single carbon atom of the triangle not connected to the C5 cycle, without other methyl group on the C3 cycle.

Thus, from the consideration of the DFT results only, it is rather difficult to say which path will be the dominant one, which justifies the need for further kinetic modeling (section 3).

Regarding the ring opening reaction, among the pathways depicted in Scheme 3, the reaction starting from 1,1-$DMCH^+$ was not calculated since this product appears in low amount experimentally. The opening of the 133-$TMCP^+$ carbocation (q) was successfully carried out, giving the r product (Scheme 4 and Figure 5). Nevertheless, the transition state is not isolated because the energy of the product is so close to the TS energy that is not possible to differentiate.

The energy of the ring opening product is as high as that of the Type B isomerization transition states (−37 kJ/mol), but its free energy is significantly lower (38 kJ/mol), reflecting the loss of the cycle strain, lowering the activation entropy for the ring opening with respect to cycle contraction and expansions. Notably, the Gibbs free energy of r (tertiary carbenium) and r* (corresponding π-complex) are very close, in agreement with previous findings for non-cyclic tertiary carbenium ions.[15]

However, the 13-$DMCH^+$ carbocation ring opening was not successfully modeled. A secondary carbocation is involved as reaction product, that always re-closed spontaneously. The simulation of non-cyclic secondary carbenium ions in zeolites by static DFT approaches was shown to be highly inaccurate.[14–19] Notably, the determination of β-scission barriers by static calculations appears to be problematic when secon-

dary carbenium ions are involved. It was indeed recently shown that performing first principles molecular dynamics is required to identify the proper transition state and account for the strong dynamic effects on the corresponding free energy barriers.[16,18] This is the reason why we did not undertake the simulation of the cracking of the ring opening products in the present work.

DFT-based microkinetic modeling

A microkinetic model considering the kinetic constants from the first principles calculations has then been built, to compare the results of the first principles calculations with the experimental data. The steps with their corresponding kinetic constants are defined in Tables S3–S5. Details are given in Supporting Information S3. Scheme 5 pictures the core of the reaction network and the concentration of the main intermediates.

The π-complexes, secondary and tertiary carbenium ions exhibiting the same skeleton are assumed to be in quasi-equilibrium and thus only one surface intermediate is considered for each product, except for the ethyl-cyclohexane skeleton where two intermediates have been used (a* and h*).

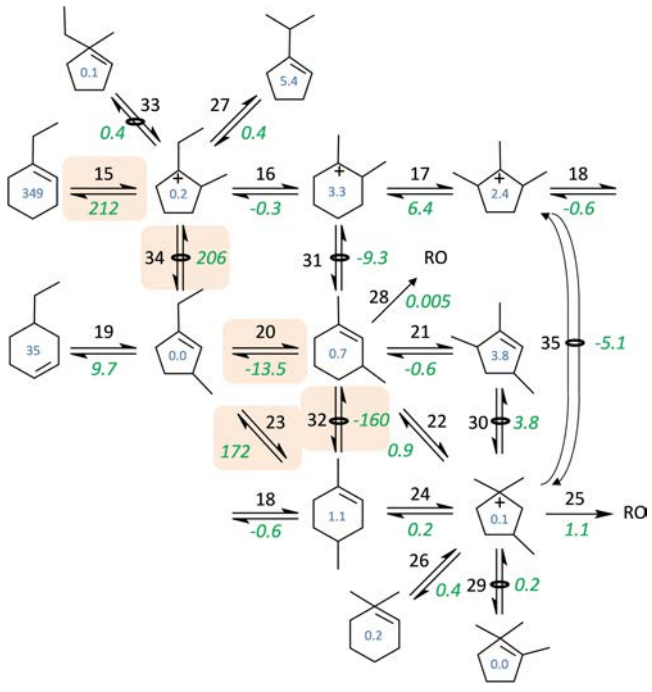

Scheme 5. Part of the reaction network for the kinetic modelling. Only surface reactions of the carbenium ions or π-complexes are shown (steps 15–35, see supporting information). The reactions are numbered in black, the net TOF (Turn Over Frequency) calculated at the reactor exit is given in green italic numbers (positive rates go from right to left and from top to bottom), the concentration of the intermediates (nanomol/kg) is given in blue. The steps underlined in light orange represent the fastest reactions. Arrows that contain the symbol ○ are quasi-equilibrated, for which $r_f/r_b = 1.00$. Step 18 on the top right continues in the middle (towards the bottom eg: 123-TMCP = 1,4-DMCH). Condition experiments, T = 285 °C, conversion equal to 68 %.

In order to reduce the number of intermediates in the model, the dehydrogenation/hydrogenation and protonation/deprotonation steps for all products are assumed to be in quasi-equilibrium and are described by an equilibrium rate constant.

The adsorption/desorption entropies and enthalpies were also calculated by DFT, but in an effort to compensate for inaccuracies in the DFT calculations, the sorption entropies were estimated by regression analysis of the complete experimental data set, while the values of the sorption enthalpies were set to the DFT values.

The isomerization and cracking thermokinetic values were fixed at their DFT values during parameter estimation, none of them was fitted. The formation of 11-DMCH and IPCP (Isopropyl-cyclopropane) were not included in the first principles study. Therefore, the parameters for the pre-exponential factors of the forward reaction were estimated by regression analysis of the experimental data. Moreover, an additional cracking path was added from the 13-DMCH intermediate (corresponding to reaction b in Scheme 3), to account for the different products inside the cracking fraction. Regarding methyl-shifts, the enthalpies of these steps were set at 0, as DFT calculations showed that the enthalpies for these steps were small, typically less than 15 kJ/mol, and the entropies were estimated by regression analysis.

The results of the modeling are shown as lines in Figures 1 and 2 and compared to the experimental features. Additional data can be found in Figure S15. Figure 1-a shows that the model fits the conversion as a function of the contact time at the three temperatures adequately. Figure 1-b shows that the isomerization *versus* cracking selectivity is also well reproduced. Figure 1-c shows that the selectivity in the various lumps of isomerization products is satisfactorily reproduced, except at low W/F_{ECH}, for which the uncertainty is high (both experimentally and computationally) due to the low conversion values. Going into the details of the composition of each lump, Figure 2 demonstrates the good performances of the model, in particular within the EMCP and DMCH families. The deviation for the TMCP family is higher, but the global selectivity for these compounds is significantly lower.

The concentration of all intermediates (Scheme 5) is very small (order of magnitude: 500 nanomol/kg) with respect to the total number of acid sites present on the catalyst (142 μmol/g, see Ref. [11]). This is in line with the very small concentration of gas phase olefins, due to the thermodynamic equilibrium for alkane dehydrogenation, which is not favorable under hydroisomerization reaction conditions (high partial pressure of hydrogen). Among these intermediates, adsorbed 1-ethylcyclohexene (a*) dominates (349 nanomol/g) followed by adsorbed 3-ethylcyclohexene (h*). Thus, the most abundant reaction intermediates are π-complexes, and not carbenium ions. However, a few carbenium ions appear in Scheme 5, meaning that they are more stable than the corresponding π-complexes, but their concentration remains lower than ethylcyclohexenes. The fastest reactions are underlined in orange in Scheme 5. This explains why 13-EMCP is the primary product, followed by 14-DMCH and 13-DMCH (in quasi-equilibrium). The route starting from 1-ethylcyclohexene dominates over that starting from 3-

ethylcyclohexene in that respect, which can be related to the very high free energy of the E transition state found by DFT (Figure 5-b). Hence, the best picture for the dominant mechanism is the following:

- First, 1-ethylcyclohexene produces 12-EMCP following Path I (Scheme 4) preferentially, due to the lower free energy of A with respect to E transition state (Figure 5).
- Then through Type A isomerization reactions, 13-EMCP is produced, that makes it possible to continue with the Path II and Path II-ter routes. In particular, the very low free energy of the F transition state is responsible for the high 14-DMCH production. This is highly interesting, as this molecule is the precursor of para-xylene, of high practical interest.[1]

This way, we can identify the critical flux of Type A isomerization reactions, that are able to connect Type B paths to follow the path dictated by the lowest free energy transition states.

The overall agreement between the model and the experiments is very good. This agreement shows that for Type B naphthene isomerization reactions, the kinetic parameters provided by first principles calculations at the channel site of the EU-1 zeolite are satisfactory. Some of the parameters were fitted and not obtained by DFT calculations, but their number is significantly reduced with respect to a fully numerical model without DFT input. Reducing the number of fitted parameters thanks to DFT calculations is thus of great help to obtain a robust and chemically relevant multi-scale kinetic model.

Conclusion

In the present work, we unravel the mechanism and the kinetics of each elementary step of the bifunctional transformation of ethylcyclohexane, considering a catalyst composed of platinum and the EU-1 zeolite. DFT calculations are key to unravel the mechanisms and relevant intermediates, but the validation of the findings comes from the comparison of the microkinetic model built from DFT calculations, and experiments.

Experimentally, the apparent reaction scheme shows the consecutive formation of ethylmethyl-cyclopentanes, dimethylcyclohexanes, and trimethylcyclopentanes as isomerization products. Ring opening also takes place as a side-reaction, followed by rapid cracking of the ring opening products.

The apparent isomerization and ring opening scheme observed experimentally has been chosen as the starting point for the DFT investigation, dealing with the acid-catalyzed steps, through carbenium intermediates. An active site located at the channel of the EU-1 zeolite was selected for this investigation. The very first reaction step involves preferentially a tertiary cyclic carbenium ion, whereas the next ones also involve secondary carbenium. The central kinetic role of the π-complexes corresponding to these secondary cations is demonstrated.

The prediction of the selectivity is made possible thanks to the DFT-based microkinetic modeling, that further includes the cracking of the ring opening products observed experimentally, with a limited number of kinetic parameters optimized by regression with respect to the experimental data. The larger part of the data comes from DFT calculations. The agreement with experimental results is very good, showing that the mechanisms proposed, the nature of the intermediates, and of the computed rate constants, are relevant. Due to the respective stability of transition states of cycle contraction-expansion steps, of Type B isomerization nature, the system dominantly evolves through the transformation of 1-ethylcyclohexene, then shifts to a second sequence of Type B isomerization reactions thanks to intercalated methyl shifts. This explains the dominant formation of 1,4-dimethylcyclohexane after re-hydrogenation. The present work is a promising implementation of DFT-based microkinetic modeling for the prediction of zeolite catalysts performances, and it opens perspectives for the more accurate simulation of ring opening and alkene cracking steps.

Experimental Section and Methods

The 1 wt.% Pt/γ-Al_2O_3–H-EU-1 catalyst was prepared and characterized as detailed in Ref. [11]. The bifunctional catalyst was obtained by mixing 20% wt of the EU-1 zeolite (Zeolyst, further transformed into its protonic form) with 80% wt of alumina loaded with 1% wt platinum. The experimental protocol is described elsewhere.[11] The mechanical mixtures were pelletized with a hydraulic press, crushed, and sieved to obtain a pellet size between 350 and 500 μm before catalytic tests.

Catalytic tests were performed in the set-up described in Ref. [11]. Total pressure (10 bar) and hydrogen to ECH molar ratio (40 mol/mol) are kept constant. According to return point, the deactivation during all the test was found to be negligible.

Periodic DFT calculations were performed with the PBE (Perdew, Burke and Ernzerhof) exchange-correlation[20] as implemented in VASP 5.3.[21] The projected augmented wave (PAW) method[22] was used to describe the core-electron interactions, and the plane wave basis set was limited to a kinetic cutoff energy of 400 eV except for the optimization of the cell dimensions, for which the cutoff was set at 800 eV. Van der Waals corrections as proposed within the D2 Grimme formalism[23] were applied. The convergence criterion for the electronic self-consistent field relaxation was fixed to 10^{-7} eV. All calculations were performed at the gamma point. The cell (Si/Al = 15, see Ref. [9]) contains exchanged $T_{10}O_{12}$, T_1O_1, and T_9O_6 sites, but the reactant molecules where placed close to the T1O1 site (in the 10MR channel).

Full geometry optimizations of the reaction intermediates were performed using a conjugate gradient algorithm, with a convergence criterion on forces of 0.005 eV.Å^{-1}. The Nudged Elastic Band (NEB) method[24] was used to locate the transition states. The number of images to investigate reaction pathways between the reactant and the product was set to 8. To start with, an interpolation scheme involving both Cartesian and internal coordinates was used (Opt'n-Path[25]). We basically perform 50 NEB steps before optimizing the structure of the highest energy image by a quasi-Newton calculation,[26] sometimes followed by a Dimer calculation.[27] Harmonic frequency calculations were performed on optimized structures (all atoms of the cell moving) with a displacement of $\pm$0.02 Å around the equilibrium atomic positions. To properly identify saddle points, most of the time some refinements of the intermediate and transition structures had to be performed, to get zero (in the case of intermediates) or only one (in the case of transition structures) imaginary frequencies. In that respect, to

eliminate spurious imaginary frequencies, line minimization methods were applied, thanks to algorithms developed by Tomáš Bučko (Univ. Bratislava).[19] For each transition structure, the connection with the expected reactants and products was established thanks to the intrinsic reaction coordinate (IRC) approach,[28] as implemented in VASP.[19] Structures identified at the end of the IRC were re-optimized with a convergence criterion on forces of 0.005 eV. $Å^{-1}$. The adsorption energy E_{ads} of all the considered species was calculated, using isolated ethylcyclohexene and the empty zeolite as references. For each of these species, the Gibbs free energy was then calculated according to the methods detailed in Ref. [9].

A microkinetic model based on the first principles results has been developed and compared to the experimental data. All the reaction steps included in the model are reported in Tables S3-S5 and correspond for the most part to the paths shown in Scheme 4. The reaction steps are grouped into three sections. The first section contains the steps starting from the gas phase species and including dehydrogenation/hydrogenation, adsorption/desorption. Protonation/deprotonation steps were only considered for the species for which the protonated form was the most stable configuration as found by first principles calculations (12-EMCP+, $12DMCP^+$, $113\text{-}TMCP^+$ and $123\text{-}TMCP^+$). The dehydrogenation / hydrogenation steps were assumed to be quasi-equilibrated. The reactor is assumed to be an isothermal plug-flow pseudo-homogeneous packed bed reactor, without any heat and mass transfer limitations. More details are given in Supporting Information S3.

Thermodynamic simulations were performed with SimSci Pro/II v 9.2 (Schneider Electric). The thermodynamic equation of state used was SRK (Soave-Redlick-Kwong). The compounds database was that from SimSCi. The equilibrium between the different compounds was evaluated with a Gibbs reactor (outlet pressure 10 bar, T between 230 and 330 °C, 50 iterations max, convergence tolerance -based on the relative change of Gibbs free energy between two iterations: 10^{-6}, Fibonacci tolerance: 0.01).

Acknowledgements

This work was performed using HPC resources from GENCI-IDRIS (Grant A0020806134) and the IFPEN ENER440 supercomputer.

Conflict of Interest

The authors declare no conflict of interest.

Keywords: alkenes · DFT · carbenium · microkinetics · zeolite

[1] C. Marcilly, *Acido-Basic Catalysis*, Technip, Paris, **2005**.
[2] J. Weitkamp, *ChemCatChem* **2012**, *4*, 292–306; C. Bouchy, G. Hastoy, E. Guillon, J. A. Martens, *Oil Gas Sci. Technol.* **2009**, *64*, 91–112; U. Olsbye, S. Svelle, M. Bjorgen, P. Beato, T. V. Janssens, F. Joensen, S. Bordiga, K. P. Lillerud, *Angew. Chem. Int. Ed* **2012**, *51*, 5810–5831; *Angew. Chem.* **2012**, *124*, 5910–5933.
[3] M. Salciccioli, M. Stamatakis, S. Caratzoulas, D. G. Vlachos, *Chem. Eng. Sci.* **2011**, *66*, 4319–4355; K. Larmier, A. Nicolle, C. Chizallet, N. Cadran, S. Maury, A.-F. Lamic-Humblot, E. Marceau, H. Lauron-Pernot, *ACS Catal.* **2016**, *6*, 1905–1920; A. Bruix, J. T. Margraf, M. Andersen, K. Reuter, *Nature Catalysis* **2019**, *2*, 659–670.
[4] M. John, K. Alexopoulos, M.-F. Reyniers, G. B. Marin, *J. Catal.* **2015**, *330*, 28–45; M. John, K. Alexopoulos, M.-F. Reyniers, G. B. Marin, *Catal. Sci. Technol.* **2017**, *7*, 1055–1072; C. Liu, R. A. van Santen, A. Poursaeidesfahani, T. J. H. Vlugt, E. A. Pidko, E. J. M. Hensen, *ACS Catal.* **2017**, *7*, 8613–8627; P. N. Plessow, A. Smith, S. Tischer, F. Studt, *J. Am. Chem. Soc.* **2019**, *141*, 5908–5915.
[5] F. Bertoncini, A. Bonduelle-Skrzypcak, J. Francis, E. Guillon, *Hydrocracking*, in: H. Toulhoat, P. Raybaud (Eds.) Catalysis by transition metal sulphides: from molecular theory to industrial applications, Editions Technip, **2013**, pp. 609–677.
[6] J. Weitkamp, S. Ernst, H. G. Karge, *Erdoel Kohle Erdgas Petrochem.* **1984**, *37*, 457–462.
[7] J. Weitkamp, P. A. Jacobs, S. Ernst, *Shape Selective Isomerization and Hydrocracking of Naphthenes Over Pt/HZSM-5 Zeolite*, in: P. A. Jacobs, N. I. Jaeger, P. Jírů, V. B. Kazansky, G. Schulz-Ekloff (Eds.) Stud. Surf. Sci. Catal., Elsevier, **1984**, pp. 279–290.
[8] M. Guisnet, *Catal. Today* **2013**, *218–219*, 123–134.
[9] E. Gutierrez-Acebo, J. Rey, C. Bouchy, Y. Schuurman, C. Chizallet, *ACS Catal.* **2019**, *9*, 1692–1704.
[10] E. Guillon, S. Lacombe, T. Sozinho, P. Magnoux, S. Gnep, P. Moreau, M. Guisnet, *Oil Gas Sci. Technol.* **2009**, *64*, 731–744.
[11] E. Gutierrez-Acebo, C. Leroux, C. Chizallet, Y. Schuurman, C. Bouchy, *ACS Catal.* **2018**, *8*, 6035–6046.
[12] P. Raybaud, A. Patrigeon, H. Toulhoat, *J. Catal.* **2001**, *197*, 98–112.
[13] D. M. Brouwer, H. Hogeveen, *Prog. Phys. Org. Chem.* **1972**, *9*, 179–240; G. G. Martens, G. B. Marin, J. A. Martens, P. A. Jacobs, G. V. Baron, *J. Catal.* **2000**, *195*, 253–267.
[14] J. Rey, A. Gomez, P. Raybaud, C. Chizallet, T. Bučko, *J. Catal.* **2019**, *373*, 361–373.
[15] J. Rey, P. Raybaud, C. Chizallet, T. Bučko, *ACS Catal.* **2019**, *9*, 9813–9828.
[16] J. Rey, C. Bignaud, P. Raybaud, T. Bucko, C. Chizallet, *Angew. Chem. Int. Ed.* **2020**, *59*, 18938–18942; *Angew. Chem.* **2020**, *132*, 19100–19104.
[17] V. Van Speybroeck, K. Hemelsoet, L. Joos, M. Waroquier, R. G. Bell, C. R. A. Catlow, *Chem. Soc. Rev.* **2015**, *44*, 7044–7111; P. Cnudde, K. De Wispelaere, J. Van der Mynsbrugge, M. Waroquier, V. Van Speybroeck, *J. Catal.* **2017**, *345*, 53–69; T. Bučko, J. Hafner, *J. Catal.* **2015**, *329*, 32–48.
[18] P. Cnudde, K. De Wispelaere, L. Vanduyfhuys, R. Demuynck, J. Van der Mynsbrugge, M. Waroquier, V. Van Speybroeck, *ACS Catal.* **2018**, *8*, 9579–9595.
[19] T. Bučko, L. Benco, J. Hafner, J. G. Ángyán, *J. Catal.* **2011**, *279*, 220–228.
[20] J. Perdew, K. Burke, M. Ernzerhof, *Phys. Rev. Lett.* **1996**, *77*, 3865–3868.
[21] G. Kresse, J. Hafner, *Phys. Rev. B* **1994**, *49*, 14251–14269; *Comput. Mater. Sci.* **1996**, *6*, 15–50.
[22] G. Kresse, D. Joubert, *Phys. Rev. B* **1999**, *59*, 1758–1775.
[23] S. Grimme, *J. Comput. Chem.* **2006**, *27*, 1787–1799.
[24] G. Henkelman, H. Jonsson, *J. Chem. Phys.* **2000**, *113*, 9978–9985.
[25] P. Fleurat-Lessard, P. Dayal, *Accessed April 2nd* **2016**.
[26] P. Pulay, *Chem. Phys. Lett.* **1980**, *73*, 393–398.
[27] G. Henkelman, H. Jónsson, *J. Chem. Phys.* **1999**, *111*, 7010–7022; A. Heyden, A. T. Bell, F. J. Keil, *J. Chem. Phys.* **2005**, *123*, 224101.
[28] K. Fukui, *Acc. Chem. Res.* **1981**, *14*, 363–368; *J. Phys. Chem.* **1970**, *74*, 4161–4163.